

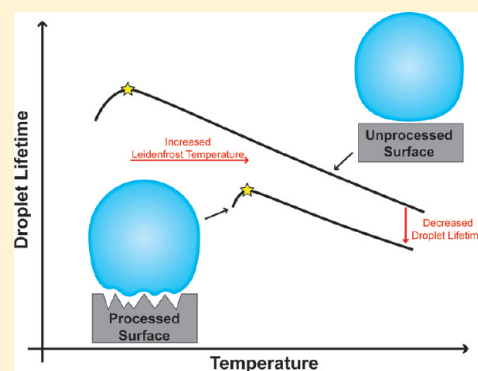
Extraordinary Shifts of the Leidenfrost Temperature from Multiscale Micro/Nanostructured Surfaces

Corey Kruse,[†] Troy Anderson,[‡] Chris Wilson,[‡] Craig Zuhlke,[‡] Dennis Alexander,[‡] George Gogos,[†] and Sidy Ndao^{*,†}

[†]Mechanical & Materials Engineering and [‡]Electrical Engineering, University of Nebraska – Lincoln, Lincoln, Nebraska, United States

Supporting Information

ABSTRACT: In the present work, the effects of surface chemistry and micro/nanostructuring on the Leidenfrost temperature are experimentally investigated. The functional surfaces were fabricated on a 304 stainless steel surface via femtosecond laser surface processing (FLSP). The droplet lifetime experimental method was employed to determine the Leidenfrost temperature for both machine-polished and textured surfaces. A precision dropper was used to control the droplet size to 4.2 μL and surface temperatures were measured by means of an embedded thermocouple. Extraordinary shifts in the Leidenfrost temperatures, as high as 175 $^{\circ}\text{C}$ relative to the polished surface, were observed with the laser-processed surfaces. These extraordinary shifts were attributed to nanoporosity, reduction in contact angle, intermittent liquid/solid contacts, and capillary wicking actions resulting from the presence of self-assembled nanoparticles formed on the surfaces. In addition to the shift in the Leidenfrost temperature, significant enhancement of the heat transfer in the film boiling regime was also observed for the laser-processed surfaces; water droplet evaporation times were reduced by up to 33% for a surface temperature of 500 $^{\circ}\text{C}$.



INTRODUCTION

When a liquid droplet is placed on a heated surface at a temperature above the saturation temperature of the liquid, the droplet evaporates in a very short amount of time as a result of very efficient nucleate boiling. Nucleate boiling is characterized by high heat transfer coefficients from the generation of vapor at a number of favored spots (nucleation sites) on the heated surface. With increasing temperature and heat flux (near the critical heat flux), the formation of more vapor in the vicinity of the surface has the effect of gradually insulating the heated surface. At high enough temperatures, these vapor pockets form a stable vapor film and result in a minimum heat flux. The corresponding temperature to this minimum heat flux is referred to as the *Leidenfrost temperature*.¹ A droplet in the Leidenfrost state is supported in a nearly frictionless state by the vapor layer.^{1–3}

Because the Leidenfrost temperature represents the maximum surface temperature at which efficient heat transfer can occur, understanding the fundamental mechanisms governing the Leidenfrost temperature is of great importance. Knowledge of these mechanisms will allow for tailoring of the Leidenfrost temperature for specific applications such as thermal management, power generation, and in drag reduction.^{4–6}

The Leidenfrost state, being an interfacial phenomenon, is expected to be governed by the chemical properties such as composition and surface energy and thermophysical properties such as density and thermal conductivity of the liquid/solid

interface in addition to the topographic (nano- and microscopic structures) characteristic of the solid surface.⁷ Earlier Leidenfrost models are based on hydrodynamic instability, homogeneous and heterogeneous metastable nucleation, thermomechanical effects, and wettability effects. These methods are summarized by Bernardin and Mudawar⁸ and were found to have relatively low accuracy in predicting the Leidenfrost temperature for various scenarios. These Leidenfrost models were developed for smooth and ideal surfaces and thus are not robust enough to accommodate complex engineered surfaces. More recent studies have identified the importance of surface roughness, surface wettability, and nanoscale porosity on predicting and shifting the Leidenfrost temperature. These parameters can be controlled by novel surface nanofabrication and chemical treatment processes. The following paragraph summarizes the literature on research efforts to control the Leidenfrost temperature.

It has been shown that the Leidenfrost temperature for a water droplet of 1.88 mm diameter on stainless steel is about 290 $^{\circ}\text{C}$.⁹ Similar Leidenfrost temperatures have also been reported in previous work.^{8–14} More recent experiments have been focused on understanding which of the above-mentioned mechanisms has the largest effect on the Leidenfrost temper-

Received: May 21, 2013

Revised: June 24, 2013

Published: June 25, 2013

ature. Contact angle and surface roughness have been shown to critically affect the Leidenfrost temperature.^{15–17} As a general trend, rendering a material more hydrophilic increases the Leidenfrost temperature and rendering a material more hydrophobic decreases the Leidenfrost temperature. Various coatings and cleaning methods have been used to modify contact angles in order to understand how these changes can shift the Leidenfrost temperature;^{4,16–19} typical Leidenfrost temperature increases were on the order of about 30 °C for superhydrophilic samples while the hydrophobic processing resulted in reductions of about 100 °C. The effects of porosity and micropost structures on the Leidenfrost temperature have also been reported. A 50% increase in porosity of an aluminum oxide surface resulted in a 45 °C increase in Leidenfrost temperature.²⁰ Adding nanopores to a SiO₂ surface resulted in a shift of 85 °C. The addition of 15 μm tall microposts to this nanoporous SiO₂ surface generated an additional increase of about 94 °C in the Leidenfrost temperature.¹⁶ Hydrophobic surfaces have also been created on stainless steel using a picosecond laser machining process. This method resulted in a contact angle of 115° and a reduction of about 120 °C in the Leidenfrost temperature.²¹

As can be seen from previous works, the Leidenfrost temperature can be shifted by modifying the surface physicochemical properties; however, an inclusive and comprehensive set of governing mechanisms has yet to be identified to fully understand the Leidenfrost phenomenon and the extent to which it can be shifted (i.e., tuned). The current experiment investigates the physicochemical properties and topographic characteristics of laser-fabricated metallic surfaces on the Leidenfrost temperature. Various surfaces were fabricated with tailored surface roughness, available interfacial area, surface wettability, and nanoporosity. In this paper, we report a new class of laser fabricated micro/nanostructured surfaces and extraordinary shifts in the Leidenfrost temperature, up to 175 °C, along with associated interfacial governing mechanisms.

EXPERIMENTAL METHODS AND THEORY

Laser Manufacturing. Multiscale surfaces (surfaces with roughness on both the micrometer and nanometer scales) are commonly applied for the fabrication of advanced wettability surfaces that range from superhydrophobic to superhydrophilic.^{22–25,39,40} Indeed, such surfaces are considered to be biologically inspired as they often mimic the surfaces of plant leaves; one iconic example is the superhydrophobic lotus leaf, which exhibits self-cleaning properties due in

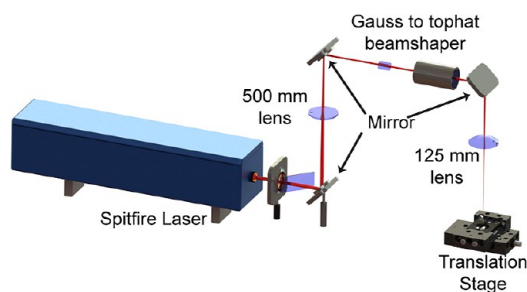


Figure 1. Schematic of the femtosecond laser surface processing (FLSP) setup. The laser power is tuned via a half waveplate and a polarizer; the beam profile is modified to a square flat-top profile via a refractive beam shaper. The sample is placed on a 3D translation stage and scanned through the path of the laser to fabricate a large area surface.

part to multiscale surface features.^{26,27} For such structured surfaces, the relative sizes of both micrometer and nanometer scale structures are critical for the control of not only the contact angle, but also the adhesion and wetting state (e.g., the fully wetting Wenzel state or the hybrid Cassie–Baxter state).^{27,28}

Femtosecond laser surface processing (FLSP) is rapidly emerging as a powerful and dynamic method for the fabrication of biologically inspired multiscale surface structures. Using this process, surfaces generally consist of self-organized, quasi-periodic micrometer-scale conical or mound structures that are covered in a layer of nanoparticles.^{29–36} These surface structures are formed through a complex combination of multiple growth mechanisms including laser ablation, capillary flow of laser-induced melt layers, and redeposition of ablated material.

A schematic of the FLSP setup is shown in Figure 1. The laser was a Ti:Sapphire (Spitfire, Spectra Physics) that produced ~50 fs pulses centered around 800 nm at a 1 kHz repetition rate. The laser power was controlled through a combination of a half waveplate and a polarizer. A refractive Gauss-to-top hat beam shaper (Eksma Optics, GTH-4–2.2FA) was used to generate a top hat beam with a square profile; this ensured that the laser fluence on the sample was uniform. The sample was placed on a computer-controlled 3D translation stage and translated through the beam path of the laser in order to process an area larger than the laser spot size. The number of pulses incident on the sample was controlled by the translation speed of the sample.

Tailoring Multiscale Surfaces. The size and shape of self-organized surface structures fabricated via FLSP are controlled through various fabrication parameters including the laser fluence, the number of laser shots per area incident on the sample, and the composition and pressure of the atmosphere during processing. In the present study, a range of multiscale surface morphologies were fabricated on 304 stainless steel and then utilized to demonstrate extraordinary shifts of the Leidenfrost temperature. The variations in the surface morphology are generated through modification of both the laser fluence and the number of pulses incident on the sample.

The fluence and shot number were chosen as control parameters as they represent two contrasting methods of controlling the total dose of laser energy transferred to a substrate. To illustrate this, consider that a given amount of laser energy can be transferred to a target substrate either through a small number of laser pulses with a large fluence or through a large number of laser pulses with a small fluence. However, the laser fluence critically impacts the laser–matter interaction mechanisms attributed to the development of multiscale structures; we recently published a shot-by-shot study of the ability of the laser fluence to influence the physical formation mechanisms of the self-organized surface structures and utilized this control to fabricate multiscale metallic surface structures that rise above the original surface.³⁶ Thus, control of the laser dose via a calculated selection of both the laser fluence and the number of pulses on the sample is a convenient method to produce a range of unique surface morphologies. A subset of this range is demonstrated in Figure 2, which documents three distinct classes of surface structures fabricated using FLSP: a new class of nanostructure-covered pyramids (NC-Pyramids), below-surface-growth mounds (BSG-mounds), and above-surface-growth mounds (ASG-mounds). The required laser fluence necessary to generate the structures increases from left to right in Figure 2.

NC-Pyramids are formed with a laser fluence near the ablation threshold with several thousand pulses, whereas both BSG-mounds and ASG-mounds are formed with laser fluence values several times the ablation threshold. Each of these surfaces comprises micrometer-scale conical structures that are covered with a layer of nanoparticles. However, the structures differ greatly in terms of the height, width, and separation of the microscale structures as well as in the thickness of the nanoparticle layer. Specifically, there are three primary mechanisms by which self-organized multiscale surface features grow in response to incident laser irradiation as depicted in Figure 3; the balance of these mechanisms is determined by the laser fluence.

The first mechanism, preferential valley ablation (PVA), is a geometry-driven process in which laser light is scattered off of defects

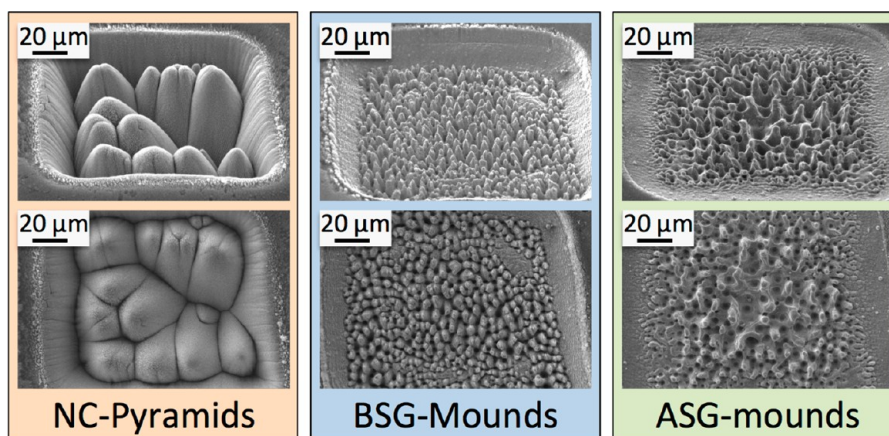


Figure 2. Scanning electron microscope images of three classes of surface morphologies fabricated by FLSP. The top image of each panel was taken at 45° to show the structure height relative to the original surface; the bottom image of each panel was taken at normal incidence to show the size and separation of the structures.

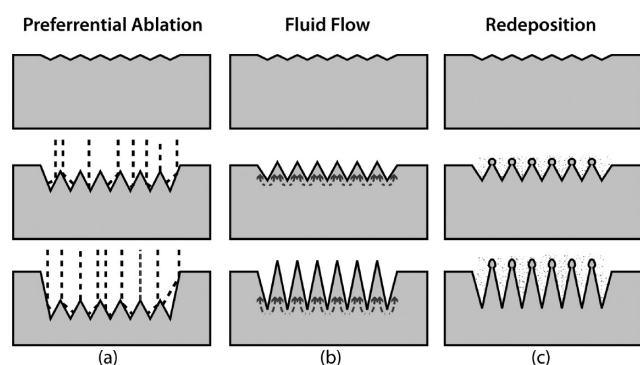


Figure 3. Schematic illustrations of three growth mechanisms leading to the development of multiscale surface features from surface precursor sites upon laser irradiation. (a) Material is ablated away around a scattering site to form structures. (b) Material is melted and flows to form structures. (c) Particles are redeposited to form structures. All three mechanisms take place in the formation of multiscale structures but the degree varies with the type of structure created.

on the sample surface that induces a higher laser fluence and thus increased ablation in the valleys between scattering sites. Upon irradiation with multiple pulses, this PVA process is the initial driving force for the formation of the microscale structures. As the structures grow, the increased subtended area of the sidewalls reduces the fluence and amplifies this effect. PVA plays an important role in the formation of all three of the surface morphologies described in Figure 2. The primary difference between NC-Pyramids and BSG-mounds is that NC-Pyramids require a defect in the material to serve as a scattering site, whereas the fluence is sufficiently high in BSG-mound creation to form surface defects via hydrodynamic ablation.^{35,37} ASG-mounds are formed with an even higher fluence, which can cause two other

formation mechanisms to occur: fluid flow of the surface melt induced by the femtosecond laser by capillary effects³⁸ and the redeposition of ablated material via vapor–liquid–solid growth.^{39–41} These two mechanisms are responsible for the upward growth of ASG-mounds. A detailed description of the development of these structures is beyond the scope of this paper; a description of the BSG-mounds and ASG-mounds is provided by Zuhlke et al.,³⁶ and a description of the NC-Pyramids is being published as a companion paper.

Surface Characterization. A polished 304 stainless steel surface sample was used as a reference and baseline for comparison to the laser-structured surfaces. This polished sample was first wet-sanded with 600 grit sandpaper and then polished to a mirror finish with the use of a series of buffing compounds.

The impact of the surface morphology as fabricated via FLSP on the Leidenfrost point was then studied with five distinct laser-processed surfaces. Each processed surface was fabricated with a different combination of laser fluence and number of laser shots in order to produce unique geometric microstructures. The fluence and shots were chosen to vary the shape and spacing of the microstructures while keeping the average height approximately constant. Table 1 highlights the various parameter values used to process each sample as well as measured surface specific characteristics of the actual sample used in testing. The separation between microstructures increases with each sample number.

A full 3D surface profile was obtained for each of the fabricated samples using a Keyence VK-X100 laser confocal microscope. From this data, the average height, surface area ratio, and surface roughness were measured. The average height represents the average peak-to-valley height of the microstructures. The surface area ratio or roughness factor⁴² is the total surface area of all the microstructures divided by the cross sectional area. The structure separation was determined through a Fast Fourier Transform (FFT) analysis of scanning electron microscope images. The contact angle was measured with a 1 μ L drop of deionized water at room temperature using a Rame-Hart Model 590 F4 Series Goniometer and Tensiometer. Contact angles were measured on 5 drops in 5 different places and

Table 1. Processing Conditions and Measured Geometric and Surface Properties

design parameters			measured parameters				
sample name	fluence (J/cm ²)	shots	average height (μ m)	surface area ratio	surface roughness (μ m R_{rms})	structure separation (μ m)	contact angle (°)
S1: BSG - Mounds	1.1	459	15	5.3	4.4	11.3	12
S2: BSG - Mounds	1.1	1359	20	5.0	5.7	11.7	5
S3: ASG - Mounds	1.4	482	15	5.0	4.5	14.1	0
S4: ASG - Mounds	1.4	1462	14	4.3	6.0	21.0	0
S5: NC - Pyramids	0.1	48703	14	3.5	5.4	24.5	15

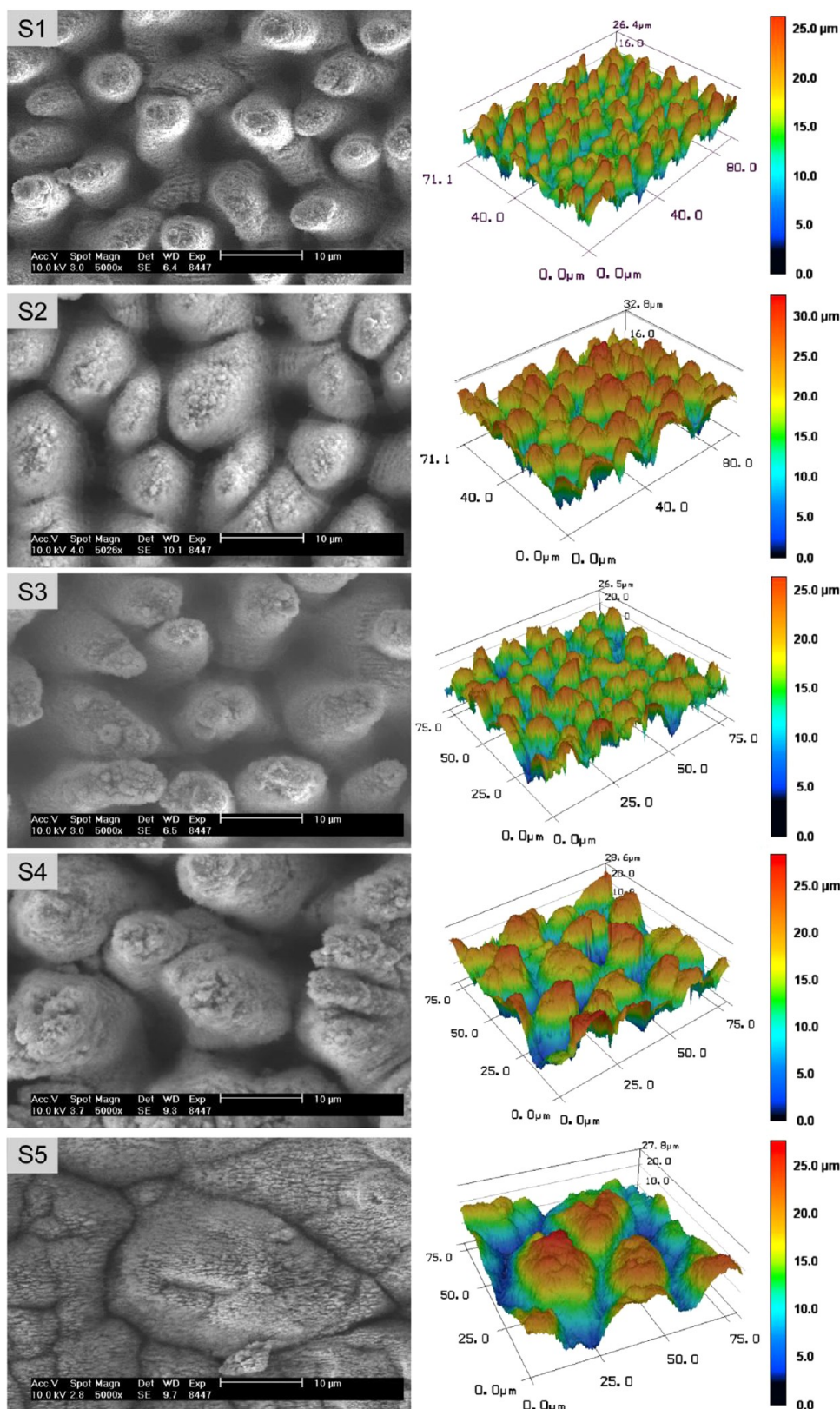


Figure 4. SEM (left panel) and 3D profile images (right panel) of the tested surfaces.

each drop was measured 10 times. This gave an average angle deviation of about 0.7° .

Figure 4 shows the SEM images and 3D profilometry scans of the unique geometric surface structures (S1 through S5) used in the Leidenfrost experiments. Samples S1 and S2 contain BSG-mounds and

are characterized by smooth round tops. Samples S3 and S4 contain ASG-mounds that were fabricated with increased laser fluence and are characterized by deep holes separating pointed structures. Sample S5 contains NC-pyramids, which are densely packed pyramidal structures fabricated with many laser pulses at a low laser fluence. The gradual

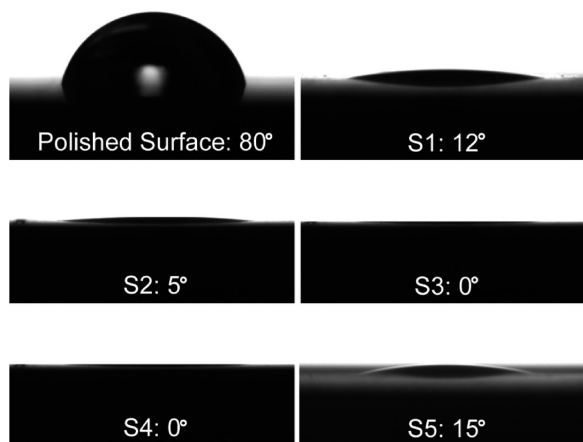


Figure 5. Contact angles of tested surfaces. The sample magnification is different to properly show the contact angle of each sample.

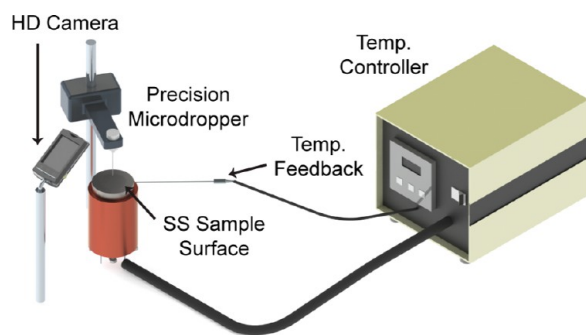


Figure 6. Leidenfrost experimental setup.

increase in structure size and separation can also be easily seen from the 3D scan images in Figure 4.

The creation of these surface micro/nanostructures also had an effect on the contact angles. The polished reference surface was found to have a contact angle of 80° . The addition of micro/nanostructures reduced the contact angle for all surfaces. Figure 5 shows the resulting contact angles for each of the surfaces. Surfaces S3 and S4 are considered “superwicking” surfaces and have a contact angle of 0° ;

videos demonstrating superwicking effect for S3 and S4 can be found in the Supporting Information. These two surfaces are similar to previously published accounts of superwicking surfaces fabricated using FLSP.^{43,44} The contact angles measured do not match angles predicted by the Wenzel model⁴² as the Wenzel model does not take into account surface chemistry and the presence of nanoparticles which promote capillary wicking which reduces the contact angle.

Leidenfrost Experiment. The method used to determine the Leidenfrost temperature was the droplet lifetime evaporation method.⁸ This method consists of placing a liquid droplet on a heated surface and measuring the evaporation time. The Leidenfrost point corresponds to the surface temperature at which the largest evaporation time occurs. A $4.2 \mu\text{L}$ (1 mm radius) deionized water droplet was chosen for this experiment in order to ensure that the radius was smaller than the capillary length ($a = (\gamma/\rho g)^{1/2}$, where γ is the surface tension, ρ is the liquid density, and g is gravitational constant). When the radius is smaller than this length, the droplet is nearly spherical when in the Leidenfrost state.² For water, the capillary length is around 2.5 mm. Droplets were also released as close to the surface as possible in order to minimize the impact velocity and corresponding Weber number ($We = \rho V^2 R / \gamma$), where V is the droplet velocity and R is the radius of the droplet.⁴⁵ Ten droplet evaporation times were recorded at each temperature and the average value was plotted. Only droplets that landed softly on the surface and remained completely intact during evaporation were considered for measurement. A Rame-Hart precision dropper was used to control the size and placement of the droplets. Figure 6 shows a CAD illustration of the Leidenfrost experimental setup.

The sample surfaces were fabricated from a 304 stainless steel block with a diameter of 64 mm and a thickness of 15 mm. Because a droplet in the Leidenfrost state tends to move around on the surface in a nearly frictionless manner, a conical depression was machined with a 1° slope and a depth of 0.4 mm at the center of the test surface in order to keep the droplet from rolling off the test area. Note that this machining step was carried out before the FLSP process. The entire conical depression was processed in order to ensure that the droplet was always on the processed surface. The sample surface temperature was controlled through the use of five cartridge heaters (Omega) implanted inside a heating block and connected to a programmable temperature controller (Rame-Hart). A K-type thermocouple was used to monitor the temperature as part of the feedback loop and was embedded 0.8 mm below the center of the conical depression. An additional thermocouple was placed on the outer edge of the conical depression to measure the uniformity of the surface temperature. The

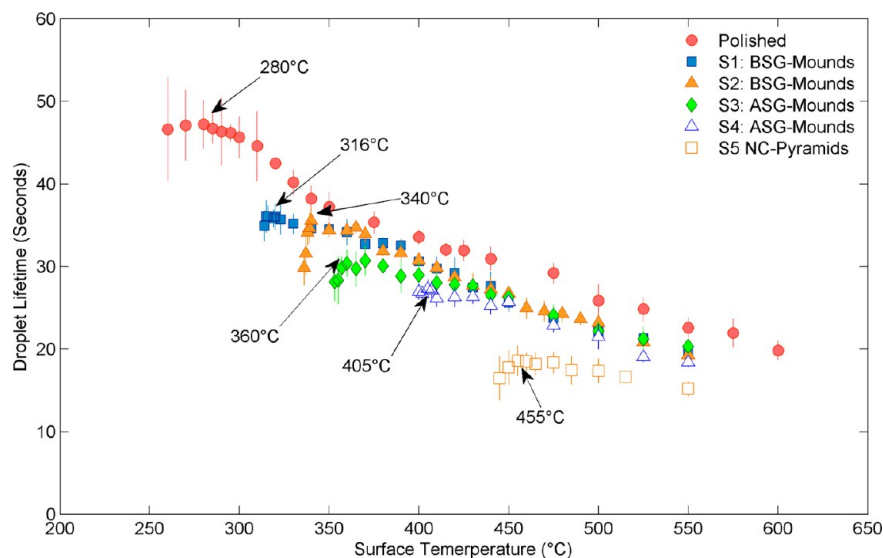


Figure 7. Droplet lifetimes with respect to surface temperature for a polished 304 stainless steel sample and five laser-processed samples with varying micro and nanostructures. The temperatures indicated with arrows are the corresponding Leidenfrost temperatures for the given surface.

temperature on the outer edge was consistently 3 °C less than the center temperature, which was less than 1% of the average operating temperatures in this experiment.

RESULTS AND DISCUSSION

Figure 7 shows the data obtained from the Leidenfrost experiments. The Leidenfrost temperature was found to be

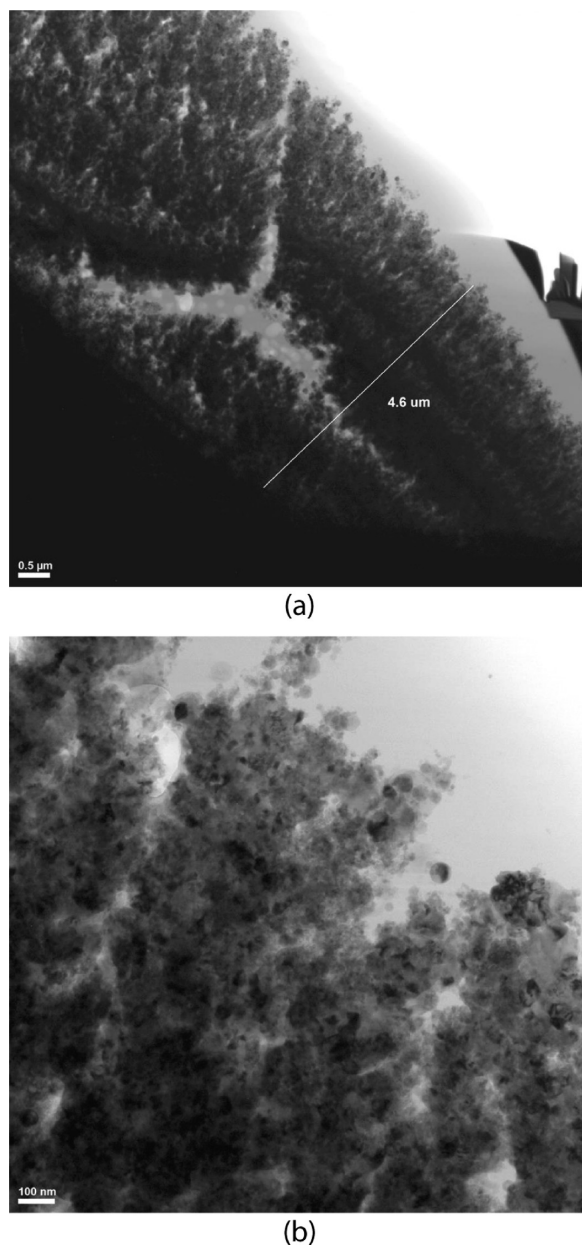


Figure 8. Transmission electron microscopy (TEM) images of a 4.6 μm -thick layer of nanoparticles that have redeposited on the NC-Pyramid structures (sample S5) during fabrication. The scale bars in the lower left corners of (a) and (b) are 0.5 μm and 100 nm, respectively. Note that the layer consists of a densely packed array of spherical nanoparticles.

280 °C for the polished surface. This number agrees well with Tamura and Tanasawa⁹ who reported a Leidenfrost temperature of 290 °C for a droplet of 1.88 mm diameter. The Leidenfrost temperature for surfaces S1, S2, S3, S4, and S5 were 316, 340, 360, 405, and 455 °C, respectively. The error bars

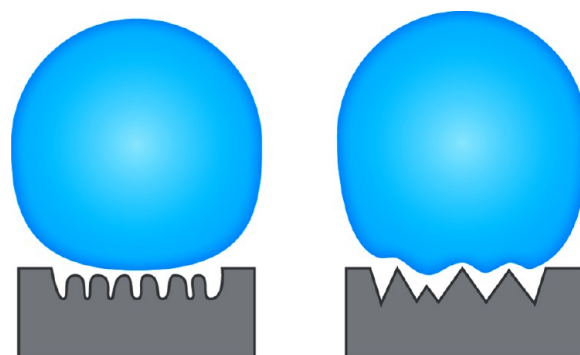


Figure 9. Schematic of the impact of nanostructure spacing on the liquid–solid interface in the film-boiling regime. As the spacing between surface structures increases, distortions in the interfacial layer can form that may lead to intermittent contact by moving droplets. The left panel represents the mound structures (S1–S4) and the right panel represents NC-pyramid structures (S5).

shown indicate the standard deviation of the ten droplet evaporation times recorded at each temperature. As can be seen from the data, extraordinary shifts in the Leidenfrost temperature, as high as 175°, have been observed for the multiscale micro/nanostructures.

An increase in the Leidenfrost temperature is typically attributed to a reduction of the contact angle, an increase in the surface roughness, or an increase in the nanoporosity.^{15–17,46} Although these properties are often interrelated, controlled experiments have indicated that each of these properties can independently affect the Leidenfrost temperature.¹⁶ Indeed, the controlled increase of the Leidenfrost temperature demonstrated by the series of surface morphologies described in Table 1 is attributed to a dynamic balance of each of these factors. For the surfaces studied here, neither the RMS surface roughness nor the surface area ratio provides a direct correlation to a controlled increase in the Leidenfrost temperature. Shifts corresponding to samples S1, S2, and S3 relative to the polished sample can be partially attributed to the gradual reduction in contact angle across this series. Further increases in the Leidenfrost temperatures for samples S4 and S5 cannot be explained by the reduction of the contact angles since the contact angle is 0° for both S3 and S4 and the 15° contact angle of S5 is the highest of any of the laser-processed surfaces. Rather, the increase in the Leidenfrost point from S3 to S4 as well as the extraordinary increase for S5 is primarily attributed to increased nanoporosity. Kim et al.¹⁶ explained that nanopores act as sites for heterogeneous bubble nucleation and therefore reduce the temperature difference required for heterogeneous nucleation, consequently resulting in an increase of the Leidenfrost temperature. The degree of nanoporosity is related to the thickness of the nanoparticle layer on the microstructure surface, which is predominantly a function of the number of pulses incident on the sample under the FLSP conditions described here since each laser pulse generates nanoparticles that can redeposit on the surface. The data in Table 1 indicates that sample S4 was fabricated with nearly 1000 more pulses per spot, equivalent to 3 times as many pulses per spot, as sample S3. Sample S5, which exhibited the largest increase in the Leidenfrost temperature, was fabricated with over 33 times as many pulses per spot as sample S4. Figure 8 shows a cross-section of the layer of nanoparticles on a NC-pyramid structure taken with a transmission electron microscope. The nanoparticle layer is greater than 4.6 μm thick on

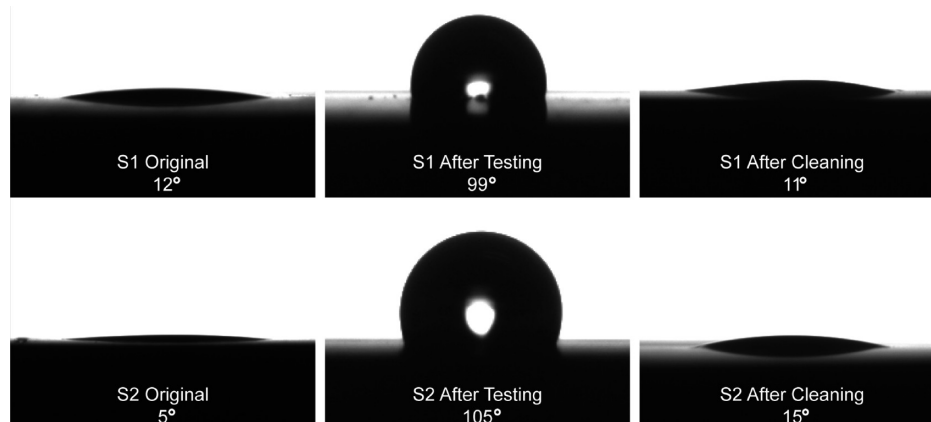


Figure 10. Contact angles of S1 and S2 several days after testing and after cleaning: (a) S1: left – original, middle – 14 days after testing, right – after cleaning, (b) S2: left – original, middle – 28 days after testing, right – after cleaning. The sample magnification is different to properly show the contact angle of each sample.

the upper portion of the NC-pyramid, which corresponds to nearly one-third of the total structure height.

The presence of these self-assembled nanoparticle layers on top of the microstructures plays a major role during intermittent solid–liquid contacts that can occur when a moving droplet interacts with the surface structures. The nanoparticles promote further wetting of the surface and heterogeneous nucleation during intermittent contact. Kim et al.¹⁶ reported that during these intermittent contacts, the velocity of the vapor generated during the heterogeneous nucleation can be greater than that of the critical velocity of the Kelvin–Helmholtz instability. When this occurs, the liquid–vapor interface can be disrupted and the stable vapor film can be destroyed, thus increasing the Leidenfrost temperature.

Intermittent contacts can result from two phenomena. First, surface microstructures may protrude into the liquid droplet when the peak to valley height is roughly equal to the vapor layer thickness. It has been reported in the literature that the vapor layer thickness can be in the range of 10–100 μm ,^{1–3,47} which is around the same range as the microstructure heights of our surfaces. This hypothesis has also been reported by Kim et al.,¹⁶ who fabricated 15 μm tall rods on the heating surface. The second way in which droplets can intermittently contact a surface occurs when the momentum of a moving droplet overcomes the resistance of the vapor film. In this case, intermittent contact between the liquid droplet and surface is more likely to occur with increased microstructure spacing as illustrated in the schematic of Figure 9 for mound structures (left) and NC-pyramid structures (right). Indeed, there is a correlation between increased microstructure separation (see Table 1) and an increase in the Leidenfrost temperature evident in Figure 7.

Indications of substantial intermittent contact between the liquid droplet and the surface were observed for sample S5; intermittent contact was manifested as brief periods in which the direction of motion of the droplet abruptly changed. A video of this sporadic motion is provided in the Supporting Information. This intermittent contact combined with nanoparticle-induced wicking generates violent heterogeneous nucleate boiling, which tends to propel droplets in different directions while increasing the Leidenfrost temperature and decreasing evaporation times above the Leidenfrost temperature.

Finally, an increase in emissivity of the laser-processed surfaces relative to the polished surfaces likely contributes to decreased droplet evaporation times by increasing radiative heat transfer. The processed surfaces have a large emissivity and appear black after processing. The emissivity of sample S2 was measured to be 0.75, whereas that of the polished surface was 0.14. At 500 °C, the evaporation time of a droplet on S1–S4 was reduced between 10 and 15% compared to the polished sample, while S5 displayed a 33% reduction in evaporation time.

Effects of Fouling on the Multiscale Nano/Microstructures. The contact angle of each surface was measured directly before Leidenfrost measurements were taken and was continually monitored throughout the measurement process, which lasted about three days for each sample. No significant changes were observed during the measurement process. After testing was completed, the samples were kept in the open environment (exposed to dust and other particulates) and the contact angles were periodically checked. The contact angles of the samples increased with environmental exposure, eventually rendering the surface hydrophobic as was also reported.⁴⁸ Figure 10 illustrates the changes in contact angle observed in S1 and S2.

The contact angle of S1 was measured 14 days after testing was completed and was found to be hydrophobic. The S2 contact angle was measured 28 days after testing was completed and was found to be slightly more hydrophobic than S1. These samples were then placed in an ultrasonic bath with isopropyl alcohol for twenty minutes, rinsed with deionized water, dried, and then the contact angle was measured again. The contact angles returned to nearly the original value as a result of cleaning. The extreme temperatures during the Leidenfrost experiments did not affect the structures on the processed sample. It was found that the contact angle change could easily be restored with simple cleaning. In applications where significant fouling can be suppressed, these structures are expected to retain their wettability.

CONCLUSION

Extraordinarily high shifts in the Leidenfrost temperature, up to 175°, have been achieved through the use of multiscale micro/nanostructures formed via femtosecond laser surface processing (FLSP). A series of laser-processed surfaces fabricated by varying laser fluence and number of shots incident on the

sample demonstrated a controlled increase in the Leidenfrost temperature. Shifts in the Leidenfrost temperature were attributed to reductions in contact angle and substantial capillary wicking due to nanoporosity during intermittent contacts of the droplet with the heated surface. The greatest shift was seen on NC-pyramid structures, which are characterized by 14 μm tall surface features separated by 25 μm that were blanketed with a thick layer of self-assembled nanoparticles. This combination of feature spacing and nanoporosity resulted in significant intermittent contact of the droplet with the surface near film boiling regime, which promoted capillary wicking and nucleate boiling. Further research is needed to determine the limits of the self-assembled nanoparticles on shifting the Leidenfrost temperature and their durability in austere environments.

■ ASSOCIATED CONTENT

■ Supporting Information

Detailed videos of the 0° contact angle and capillary wicking, the droplet motion during evaporation on S4, and the droplet motion during evaporation on S5. This material is available free of charge via the Internet at <http://pubs.acs.org>.

■ AUTHOR INFORMATION

Corresponding Author

*E-mail: sndao2@unl.edu.

Notes

The authors declare no competing financial interest.

■ ACKNOWLEDGMENTS

This work has been supported by a grant through the Nebraska Center for Energy Sciences Research (NCESR) with funds provided by Nebraska Public Power District (NPPD) to the University of Nebraska – Lincoln (UNL) No. 4200000844, by funds from the Air Force Research Laboratory (AFRL) High Energy Laser-Joint Technology Office (HEL-JTO) No. FA9451-12-D-019/0001, JTO Number: 12-BAA-0467, and by funds from the Department of Mechanical and Materials Engineering and the College of Engineering at UNL, awarded to S.N.

■ REFERENCES

- (1) Zhang, S.; Gogos, G. Film evaporation of a spherical droplet over a hot surface: fluid mechanics and heat/mass transfer analysis. *J. Fluid Mech.* **1991**, *222*, 543–563.
- (2) Bianca, A.; Clanet, C.; Quéré, D. Leidenfrost drops. *Phys. Fluids* **2003**, *15*, 1632–1637.
- (3) Burton, J.; Sharpe, A.; van der Veen, R.; Franco, A.; Nagel, S. Geometry of the vapor layer under a Leidenfrost drop. *Phys. Rev. Lett.* **2012**, *109*, 074301.
- (4) Vakarelski, I.; Patankar, N.; Marston, J.; Chan, D.; Thoroddsen, S. Stabilization of Leidenfrost vapour layer by textured superhydrophobic surfaces. *Nature* **2012**, *489* (7415), 274–277.
- (5) Linke, H.; Alemán, B.; Melling, L.; Taormina, M.; Francis, M.; Dow-Hygelund, C.; Stout, A. Self-propelled Leidenfrost droplets. *Phys. Rev. Lett.* **2006**, *96* (15), 154502.
- (6) Vakarelski, I.; Marston, J.; Chan, D.; Thoroddsen, S. Drag reduction by Leidenfrost vapor layers. *Phys. Rev. Lett.* **2011**, *106*, 214501.
- (7) Carey, V. P. *Liquid-vapor phase-change phenomena*; Taylor and Francis, 1992.
- (8) Bernardin, J.; Mudawar, I. The Leidenfrost point: experimental study and assessment of existing models. *Transactions-American Society of Mechanical Engineers Journal of Heat Transfer* **1999**, *121*, 894–903.

- (9) Tamura, Z.; Tanasawa, Y. Evaporation and combustion of a drop contacting with a hot surface. *Symposium (International) on Combustion* **1958**, *7*, 509–522.

- (10) Godleski, E.; Bell, K. The Leidenfrost phenomenon for binary liquid solutions; Doctoral dissertation; Oklahoma State University, 1967.

- (11) Patel, B. M.; Bell, K. J. The Leidenfrost phenomenon for extended liquid masses; Doctoral dissertation; Oklahoma State University, 1965.

- (12) Baumeister, K.; Henry, R.; Simon, F. Role of the Surface in the Measurement of the Leidenfrost Temperature, In *Augmentation of Convective Heat and Mass Transfer*, Bergles, A. E.; Webb, R. L., Eds.; ASME: New York, 1970; pp 91–101.

- (13) Emmerson, G. The effect of pressure and surface material on the Leidenfrost point of discrete drops of water. *Int. J. Heat Mass Transfer* **1975**, *18* (3), 381–386.

- (14) Xiong, T.; Yuen, M. Evaporation of a liquid droplet on a hot plate. *Int. J. Heat Mass Transfer* **1991**, *34* (7), 1881–1894.

- (15) Nagai, N.; Nishio, S. Leidenfrost temperature on an extremely smooth surface. *Experimental Thermal and Fluid Science* **1996**, *12* (3), 373–379.

- (16) Kim, H.; Truong, B.; Buongiorno, J.; Hu, L. On the effect of surface roughness height, wettability, and nanoporosity on Leidenfrost phenomena. *Appl. Phys. Lett.* **2011**, *98* (8), 083121–083121.

- (17) Hughes, F. The evaporation of drops from super-heated nano-engineered surfaces; Doctoral dissertation; Massachusetts Institute of Technology, 2009.

- (18) Takata, Y.; Hidaka, S.; Yamashita, A.; Yamamoto, H. Evaporation of water drop on a plasma-irradiated hydrophilic surface. *International Journal of Heat and Fluid Flow* **2004**, *25* (2), 320–328.

- (19) Munoz, R.; Beving, D.; Yan, Y. Hydrophilic zeolite coatings for improved heat transfer. *Ind. Eng. Chem. Res.* **2005**, *44*, 4310–4315.

- (20) Huang, C.; Carey, V. The effects of dissolved salt on the Leidenfrost transition. *Int. J. Heat Mass Transfer* **2007**, *50* (1), 269–282.

- (21) Arnaldo del Cerro, D.; Marin, A.; Romer, G.; Pathiraj, B.; Lohse, D.; Huis in 't Veld, A. Leidenfrost point reduction in micro-patterned metallic surfaces. *Langmuir* **2012**, *28*, 15106–15110.

- (22) Bizi-Bandoki, P.; Benayoun, S.; Valette, S.; Beaugiraud, B.; Audouard, E. Modifications of roughness and wettability properties of metals induced by femtosecond laser treatment. *Appl. Surf. Sci.* **2011**, *257* (12), 5213–5218.

- (23) Wang, Z.; Zheng, H.; Xia, H. Femtosecond laser-induced modification of surface wettability of PMMA for fluid separation in microchannels. *Microfluid. Nanofluid.* **2011**, *10* (1), 225–229.

- (24) Wu, J.; Xia, J.; Lei, W.; Wang, B. A one-step method to fabricate lotus leaves-like ZnO film. *Mater. Lett.* **2011**, *65* (3), 477–479.

- (25) Baldacchini, T.; Carey, J.; Zhou, M.; Mazur, E. Superhydrophobic surfaces prepared by microstructuring of silicon using a femtosecond laser. *Langmuir* **2006**, *22* (11), 4917–4919.

- (26) Koch, K.; Bhushan, B.; Jung, Y.; Barthlott, W. Fabrication of artificial Lotus leaves and significance of hierarchical structure for superhydrophobicity and low adhesion. *Soft Matter* **2009**, *5* (7), 1386–1393.

- (27) Stratakis, E.; Ranella, A.; Fotakis, C. Biomimetic micro/nanostructured functional surfaces for microfluidic and tissue engineering applications. *Biomicrofluidics* **2011**, *5*, 013411.

- (28) Feng, L.; Zhang, Y.; Xi, J.; Zhu, Y.; Wang, N.; Xia, F.; Jiang, L. Petal effect: a superhydrophobic state with high adhesive force. *Langmuir* **2008**, *24*, 4114–4119.

- (29) Tull, B.; Carey, J.; Mazur, E.; McDonald, J.; Yalisove, S. Silicon surface morphologies after femtosecond laser irradiation. *MRS Bull.* **2006**, *31*, 626–633.

- (30) Wu, B.; Zhou, M.; Li, J.; Ye, X.; Li, G.; Cai, L. Superhydrophobic surfaces fabricated by microstructuring of stainless steel using a femtosecond laser. *Appl. Surf. Sci.* **2009**, *256*, 61–66.

- (31) Nayak, B.; Gupta, M.; Kolasinski, K. Spontaneous formation of nanospiked microstructures in germanium by femtosecond laser irradiation. *Nanotechnology* **2007**, *18*, 195302.

- (32) Nayak, B.; Gupta, M. Ultrafast laser-induced self-organized conical micro/nano surface structures and their origin. *Optics and Lasers in Engineering* **2010**, *48*, 966–973.
- (33) Her, T.; Finlay, R.; Wu, C.; Mazur, E. Femtosecond laser-induced formation of spikes on silicon. *Appl. Phys. A: Mater. Sci. Process.* **2000**, *70*, 383–385.
- (34) Yong Hwang, T.; Guo, C. Polarization and angular effects of femtosecond laser-induced conical microstructures on Ni. *J. Appl. Phys.* **2012**, *111*, 083518–083518.
- (35) Vorobyev, A.; Guo, C. Direct femtosecond laser surface nano/microstructuring and its applications. *Laser & Photonics Reviews* **2012**, DOI: 10.1002/lpor.201200017.
- (36) Zuhlke, C.; Anderson, T.; Alexander, D. Formation of multiscale surface structures on nickel via above surface growth and below surface growth mechanisms using femtosecond laser pulses. *Opt. Express* **2013**, *21*, 8460–8473.
- (37) Tsiibidis, G.; Barberoglou, M.; Loukakos, P.; Stratakis, E.; Fotakis, C. Dynamics of ripple formation on silicon surfaces by ultrashort laser pulses in subablation conditions. *Phys. Rev. B* **2012**, *86*, 115316.
- (38) Sanchez, F.; Morenza, J.; Trtik, V. Characterization of the progressive growth of columns by excimer laser irradiation of silicon. *Appl. Phys. Lett.* **1999**, *75*, 3303–3305.
- (39) Crouch, C.; Carey, J.; Warrender, J.; Aziz, M.; Mazur, E.; Génin, F. Comparison of structure and properties of femtosecond and nanosecond laser-structured silicon. *Appl. Phys. Lett.* **2004**, *84*, 1850–1852.
- (40) Dolgaev, S.; Lavrishev, S.; Lyalin, A.; Simakin, A.; Voronov, V.; Shafeev, G. Formation of conical microstructures upon laser evaporation of solids. *Appl. Phys. A: Mater. Sci. Process.* **2001**, *73*, 177–181.
- (41) Pedraza, A.; Fowlkes, J.; Lowndes, D. Self-organized silicon microcolumn arrays generated by pulsed laser irradiation. *Appl. Phys. A: Mater. Sci. Process.* **1999**, *69*, 731–734.
- (42) Wenzel, R. Surface Roughness and Contact Angle. *J. Phys. Chem.* **1949**, *53*, 1466–1467.
- (43) Vorobyev, A.; Guo, C. Metal pumps liquid uphill. *Appl. Phys. Lett.* **2009**, *94*, 224102–224102.
- (44) Vorobyev, A.; Guo, C. Laser turns silicon superwicking. *Opt. Express* **2010**, *18*, 6455–6460.
- (45) Tran, T.; Staat, H.; Prosperetti, A.; Sun, C.; Lohse, D. Drop impact on superheated surfaces. *Phys. Rev. Lett.* **2012**, *108*, 036101.
- (46) Avedisian, C.; Koplík, J. Leidenfrost boiling of methanol droplets on hot porous/ceramic surfaces. *Int. J. Heat Mass Transfer* **1987**, *30*, 379–393.
- (47) Quéré, D. Leidenfrost Dynamics. *Annu. Rev. Fluid Mech.* **2013**, *45*, 197–215.
- (48) Kietzig, A.; Hatzikiriakos, S.; Englezos, P. Patterned superhydrophobic metallic surfaces. *Langmuir* **2009**, *25*, 4821–4827.